Composite Structures 305 (2023) 116409

Contents lists available at ScienceDirect

Composite Structures

journal homepage: www.elsevier.com/locate/compstruct

Material uncertainty quantification for optimized composite structures with failure criteria

Dženan Hozić [a,b,*], Carl-Johan Thore [b], Christopher Cameron [a], Mohamed Loukil [c]

[a] RISE Research Institutes of Sweden, Division of Materials and Production, Polymers, Fibers and Composites Department, Box 857, 501 15 Borås, Sweden
[b] Linköping University, Division of Solid Mechanics, SE 581 83 Linköping, Sweden
[c] Linköping University, Division of Engineering Materials, SE 581 83 Linköping, Sweden

ARTICLE INFO

Keywords:
Laminated composites
Structural optimization
Hyperbolic function parametrization (HFP)
Robust optimization
Uncertainty quantification
Material uncertainty

ABSTRACT

We propose a method to analyze effects of material uncertainty in composite laminate structures optimized using a simultaneous topology and material optimization approach. The method is based on computing worst-case values for the material properties and provides an efficient way of handling variation in material properties of composites for stiffness driven optimization problems. An analysis is performed to evaluate the impact of material uncertainty on designs from two design problems: Maximization of stiffness and minimization of a failure criteria index, respectively. The design problems are solved using different loads, boundary conditions and manufacturing constraints. The analysis indicates that the influence of material uncertainty is dependent on the type of optimization problem. For compliance problems the impact on the objective value is proportional to the changes of the constitutive properties and the effect of material uncertainty is consistent and predictable for the generated designs. The strength-based problem shows that material uncertainty has a significant impact on the response, and the effects of material uncertainty is not consistent and changes for different design requirements. In addition, the results show an increase of up to 25% of the maximum failure index when considering the worst-case deviation of the constitutive properties from their nominal values.

1. Introduction

Structural design of high-performance composite structures needs to consider many aspects to be successful. Even for moderate-sized design problems this requires handling of a large number of material, design and manufacturing parameters. Structural optimization (SO) is often used to efficiently handle these parameters and obtain composite structures with maximized performance. However, optimality often comes at the cost of robustness of the design. That is, optimizing for one loading scenario, or a fixed set of material properties and so on, implies sacrificing performance for others. Therefore, it is important to investigate the robustness of optimized structures due to variability, i.e. uncertainty, in the input data of the optimization problem. It is well-known that composite materials can exhibit significant variations of the material properties due to e.g. material constituent production, composite material production (e.g. pre-preg, fabrics, tow, etc.), composite manufacturing techniques or material testing and evaluation methodologies [1–3].

Methods to include uncertainty in SO are often classified as stochastic/ probabilistic or deterministic/worst-case [4]. Stochastic methods have been the primary focus of research efforts [5], and are divided into two groups, both relying on detailed knowledge of probability distributions of the uncertainty data. The first group is referred to as robust design optimization (RDO) [6,7], where statistical moments (mean value and variances) are considered as objectives or constraints. The second group is the so-called reliability-based design optimization (RBDO) [8–13], where the functionals relate to the probabilities of failure, approximately quantified using reliability indices. Deterministic methods deal with worst-case design scenarios, where a structure is optimized to withstand the worst possible input data regardless of its probability. In contrast to stochastic methods, much less research work exist on worst-case methods in regards of handling material uncertainty in SO problems, and the primary focus has been on isotropic materials [14–17].

Except in some special cases, such as stiffness variation for uncertain Young's and shear modulii (see Appendix B), computing the worst-case is a challenging, non-convex optimization problem. Depending on the model response studied and the parametrization of the uncertainty, it is sometimes possible to solve it numerically to global optimality [18,19]

* Corresponding author at: RISE Research Institutes of Sweden, Division of Materials and Production, Polymers, Fibers and Composites Department, Box 857, 501 15 Borås, Sweden.
E-mail address: dzenan.hozic@ri.se (D. Hozić).

https://doi.org/10.1016/j.compstruct.2022.116409
Received 27 April 2022; Received in revised form 19 September 2022; Accepted 24 October 2022
Available online 11 November 2022

with reasonable cost. In principle, global optimization methods such as branch-and-bound can always be used to compute solutions whose optimal value (the worst response) is within a user-specified distance from the true worst-case, but in practice such methods are extremely computationally demanding (even for the case of load-uncertainty [20] which is much cheaper than material uncertainty because the stiffness matrix is constant). Genetic algorithms and alike have been touted as a way to compute globally optimal solutions (convergence to a globally optimal solution is guaranteed in the limit of visiting every point in the feasible set), but the large number of function evaluation typically required makes such methods impractical for our application [21], and unlike for branch-and-bound methods no estimate of the distance to the true solution is given. A different approach to the worst-case problem is to replace it with some convex problem which is guaranteed to overestimate the worst-case; the main difficulties being the construction of such a convex problem and to quantify the overestimation.

In the present work, we perform an uncertainty quantification (UQ) [22] of composite material properties to investigate their influence on the performance of optimized composite structures. A UQ quantifies the sensitivity of model/system output parameters, such as structural responses, to the variability of input parameters such as material properties. UQ problems are often treated using a probabilistic approach [23]. We apply a deterministic approach to handle UQ problems, where the idea is to compute the worst possible values for the uncertain material parameters as they vary in a conservative envelope defined by simple lower and upper bounds. Towards this end, we propose a pragmatic approach to the problem of finding the worst-case values for material parameters based on treating the worst-case problem using local optimization solvers. Although there is no guarantee of global optimality using such solvers, our numerical experiments indicate that this approach is fast and robust. The local solver can also be combined with a multi-start strategy, or the tunneling and deflation approaches of [24] and [25] respectively, for improved robustness.

We remark that much work on SO under material uncertainty have used compliance as the performance measure. However, recent results [18,26] suggest that the designs of structures optimized for compliance under material uncertainty differ little, if at all from structures optimized under nominal conditions. This emphasizes the necessity to evaluate other types of stiffness driven responses under material uncertainty, such as composite failure criteria as studied herein, but also for example modal responses, buckling, and aeroelastic responses.

2. Composite parametrization

The current work uses a versatile discrete parametrization technique that enables simultaneous material and topology optimization of composite laminate structures, referred to as Hyperbolic Function Parametrization (HFP) [27]. HFP relies on efficient filtering and penalization of intermediate values of the continuous *numerical* design variables to generate sets of discrete *physical* design variables, that are used to evaluate composite designs. In the current work, a new functionality is added to HFP that include uncertainty parametrization for material properties of composites.

2.1. Design parametrization

2.1.1. Stiffness properties

Considering a composite laminate consisting of n_l plies, the design domain Ω is divided into n_e finite elements (FEs), such that the domain Ω_{el} represents the volume occupied by the l:th ply in the e:th element. The parametrization of the stiffness properties are performed on a ply level, for which the effective constitutive property matrix $\boldsymbol{E}_{el}$ is given by the interpolation function

$$\boldsymbol{E}_{el} = \boldsymbol{E}_{el}(\tilde{\boldsymbol{\rho}}, \tilde{\boldsymbol{x}}, \boldsymbol{\xi}) = \boldsymbol{E}_0 + v_{el}(\tilde{\boldsymbol{\rho}}) \sum_{c=1}^{n_c} \omega_{elc}(\tilde{\boldsymbol{x}})(\boldsymbol{E}_c(\boldsymbol{\xi}) - \boldsymbol{E}_0), \quad \forall\,(e,l). \tag{1}$$

Here v_{el} and ω_{elc} are penalization functions that operate on the physical ply density ($\tilde{\rho}$) and candidate material ($\tilde{x}$) variables, respectively. These variables in turn are obtained from the optimization variables $\boldsymbol{\rho}$ and $\boldsymbol{x}$ through in-plane and out-of-plane filtering; see [27] for details. Furthermore, n_c is the total number of candidate materials, $\boldsymbol{E}_c(\boldsymbol{\xi})$ is the constitutive matrix of a candidate material c expressed using a set of uncertainty variables $\boldsymbol{\xi}$. The positive definite matrix $\boldsymbol{E}_0 \prec \boldsymbol{E}_c$ is introduced to ensure that $\boldsymbol{E}_{el}$ is positive definite for every admissible design.

The uncertainty variables $\boldsymbol{\xi}$ are associated to the independent components of $\boldsymbol{E}_c(\boldsymbol{\xi})$. Here it is assumed that the uncertainty variables can vary arbitrary within a conservative envelope defined by a upper and lower bound. They are thus confined to the convex and compact set

$$\mathcal{M} = \left\{ \boldsymbol{\xi} \in \mathbb{R}^{n_\xi} \,\middle|\, \underline{\xi_n} \le \xi_n \le \overline{\xi_n}, \quad \forall\, n \right\}, \tag{2}$$

where n_ξ is the number of uncertainty variables and the limits are given by

$$\underline{\xi_n} = 1 - \delta_n, \quad \overline{\xi_n} = 1 + \delta_n, \quad \forall\, n.$$

Here δ_n is the fraction of variation of each independent property of the constitutive matrix. The limits of ξ_n in (2) are defined such that $\xi_n = 1$ represents the nominal value of the corresponding material property.

The constitutive matrix $\boldsymbol{E}_c(\boldsymbol{\xi})$ is, assuming orthotropic material properties, given by [28]

$$\boldsymbol{E}_c(\boldsymbol{\xi}) = \boldsymbol{T}_c \boldsymbol{C}(\boldsymbol{\xi}) \boldsymbol{T}_c^{\mathrm{T}}, \quad \forall\, c \tag{3}$$

where $\boldsymbol{E}_c(\boldsymbol{\xi})$ is given in the global problem frame of reference (P-frame), while $\boldsymbol{C}(\boldsymbol{\xi})$ is given in the local material frame of reference (M-frame). The transformation matrix $\boldsymbol{T}_c$ transforms the constitutive properties between the two frames and is defined as

$$\boldsymbol{T}_c = \begin{pmatrix} c^2 & s^2 & 0 & 0 & -2sc \\ s^2 & c^2 & 0 & 0 & 2sc \\ 0 & 0 & c & s & 0 \\ 0 & 0 & -s & c & 0 \\ sc & -sc & 0 & 0 & c^2\text{-}s^2 \end{pmatrix}, \tag{4}$$

where $c = \cos\theta_c$, $s = \sin\theta_c$ and θ_c is the fiber orientation of a candidate material. $\boldsymbol{T}_c$ is defined based on First-Order Shear Deformation Theory (FSDT) [28] that is assumed to govern the mechanical behavior of the composite laminates in the current work. The matrix $\boldsymbol{C}(\boldsymbol{\xi})$ in (3) is given by

$$\boldsymbol{C}(\boldsymbol{\xi}) = \begin{pmatrix} C_{11}(\boldsymbol{\xi}) & C_{12}(\boldsymbol{\xi}) & 0 & 0 & 0 \\ C_{12}(\boldsymbol{\xi}) & C_{22}(\boldsymbol{\xi}) & 0 & 0 & 0 \\ 0 & 0 & C_{44}(\boldsymbol{\xi}) & 0 & 0 \\ 0 & 0 & 0 & C_{55}(\boldsymbol{\xi}) & 0 \\ 0 & 0 & 0 & 0 & C_{66}(\boldsymbol{\xi}) \end{pmatrix}, \tag{5}$$

where the non-zero components are defined as

$$\begin{aligned} C_{11}(\boldsymbol{\xi}) &= \frac{E_1(\boldsymbol{\xi})}{1 - \nu_{12}(\boldsymbol{\xi})\nu_{21}(\boldsymbol{\xi})}, & C_{12}(\boldsymbol{\xi}) &= \frac{\nu_{12}(\boldsymbol{\xi})E_2(\boldsymbol{\xi})}{1 - \nu_{12}(\boldsymbol{\xi})\nu_{21}(\boldsymbol{\xi})}, \\ C_{22}(\boldsymbol{\xi}) &= \frac{E_2(\boldsymbol{\xi})}{1 - \nu_{12}(\boldsymbol{\xi})\nu_{21}(\boldsymbol{\xi})}, & C_{44}(\boldsymbol{\xi}) &= G_{23}(\boldsymbol{\xi}), \\ C_{55}(\boldsymbol{\xi}) &= G_{13}(\boldsymbol{\xi}), & C_{66}(\boldsymbol{\xi}) &= G_{12}(\boldsymbol{\xi}). \end{aligned} \tag{6}$$

These components are governed by six ($n_\xi = 6$) independent material properties: Young's modulii E_1, E_2, shear modulii G_{12}, G_{23}, G_{13} and major Poisson's ratio ν_{12}. The interdependent minor Poisson's ratio ν_{21} in (6) is given as

$$\nu_{21}(\boldsymbol{\xi}) = \nu_{12}(\boldsymbol{\xi}) \frac{E_2(\boldsymbol{\xi})}{E_1(\boldsymbol{\xi})}.$$

The independent material properties are parametrized according to

$$\begin{aligned} E_1(\boldsymbol{\xi}) &= \xi_1 E_1^{\mathrm{N}}, & E_2(\boldsymbol{\xi}) &= \xi_2 E_2^{\mathrm{N}}, & \nu_{12}(\boldsymbol{\xi}) &= \xi_3 \nu_{12}^{\mathrm{N}}, \\ G_{23}(\boldsymbol{\xi}) &= \xi_4 G_{23}^{\mathrm{N}}, & G_{13}(\boldsymbol{\xi}) &= \xi_5 G_{13}^{\mathrm{N}}, & G_{12}(\boldsymbol{\xi}) &= \xi_6 G_{12}^{\mathrm{N}}, \end{aligned} \tag{7}$$

where a superscript N indicates a nominal value.

2.1.2. Strength properties

The strength properties of a composite laminate are evaluated using strain-and stress-based failure criteria which are further discussed in Section 3. In the context of composite design optimization, a parametrization of the failure criteria based on the computation of an effective failure index is proposed by Lund [29], of the form

$$\mathcal{F}_{el}^{\text{eff}}(\tilde{\rho},\tilde{\mathbf{x}},\boldsymbol{\xi}) = \sum_{c=1}^{n_c} \psi_{elc}(\tilde{\rho},\tilde{\mathbf{x}})\mathcal{F}_{elc}(\tilde{\rho},\tilde{\mathbf{x}},\boldsymbol{\xi}). \tag{8}$$

Here $\mathcal{F}_{elc}$ is the failure index for candidate material c of a ply l in element e, and the penalization function

$$\psi_{elc}(\tilde{\rho},\tilde{\mathbf{x}}) = \frac{\tilde{\rho}_{el}}{1+r(1-\tilde{\rho}_{el})}\frac{\tilde{x}_{elc}}{1+r(1-\tilde{x}_{elc})}, \quad \forall\,(e,l,c) \tag{9}$$

where the penalization factor r is set such that an above-linear penalization of the intermediate values of the physical design variables $(\tilde{\rho},\tilde{\mathbf{x}})$ is achieved. This will, depending on the optimization problem formulation, make $\mathcal{F}_{elc}$ disproportionately expensive for intermediate values of $(\tilde{\rho},\tilde{\mathbf{x}})$.

3. Composite failure criteria

Composite failure criteria is a critical analysis tool used to evaluate and understand the mechanical behavior of a composite structure. It enables the prediction of the structural behavior and durability of a structure subjected to arbitrary loads. The evaluation is performed on a composite ply level by computing a failure index $\mathcal{F}_l$ using stresses exerted on ply l and checking that the failure index is below the failure limit, i.e. $\mathcal{F}_l \leq 1$. A failure index $\mathcal{F}_l > 1$ indicates that the stresses exerted on the ply are above the strength limits of the material, which can lead to activation of various composite failure modes.

Failure of a composite laminate (damage) can be divided into three distinct phases [30]:

- *Elastic phase* - Stresses exerted on the composite plies are not sufficient to result in damage.
- *Failure initiation phase* - Stresses are sufficient to initiate damage by activation of one or more failure modes.
- *Post failure phase* - Characterization and estimation of damage propagation of activated failure modes.

Numerous composite failure criteria have been developed over the years. Some are more general and can be applied across multiple phases, while others have a narrow focus for their application and are better suited to characterize specific damage phases. Therefore, not all failure criteria are suited to evaluate an arbitrary composite design, and the choice of failure criteria should reflect the requirements and complexity of the design intent.

In the present work the design intent is to generate composite laminate designs that retain mechanical behavior within the elastic phase. For this purpose we have chosen to implement the Tensor Polynomial Criterion, commonly know as the Tsai–Wu failure criteria [31], for evaluation of mechanical behavior of the composite laminate. Following the notation introduced in Section 2, based on FSDT, the Tsai–Wu failure criteria for orthotropic materials is given by

$$\begin{aligned}\mathcal{F}_{elc}(\tilde{\rho},\tilde{\mathbf{x}},\boldsymbol{\xi}) \quad &= F_1\sigma_1 + F_2\sigma_2 + 2F_{12}\sigma_1\sigma_2 \\ &+ F_{11}\sigma_1^2 + F_{22}\sigma_2^2 + F_{44}\sigma_4^2 + F_{55}\sigma_5^2 + F_{66}\sigma_6^2 \leq 1\end{aligned} \tag{10}$$

where F_i and F_{ij} are strength components given by

$$\begin{aligned} F_1 &= \frac{1}{\mathrm{X_t}} - \frac{1}{\mathrm{X_c}}, & F_2 &= \frac{1}{\mathrm{Y_t}} - \frac{1}{\mathrm{Y_c}}, & F_{12} &= -\frac{1}{2}\frac{1}{\sqrt{\mathrm{X_tX_cY_tY_c}}}, \\ F_{11} &= \frac{1}{\mathrm{X_tX_c}}, & F_{22} &= \frac{1}{\mathrm{Y_tY_c}}, & F_{44} &= \frac{1}{\mathrm{Q}^2}, \\ F_{55} &= \frac{1}{\mathrm{R}^2}, & F_{66} &= \frac{1}{\mathrm{S}^2}, \end{aligned} \tag{11}$$

in which $\mathrm{X_t}, \mathrm{X_c}$ and $\mathrm{Y_t}, \mathrm{Y_c}$ are the tensile and compressive strength properties along the 1- and 2-axis of the ply, respectively. The parameters Q and R are the transversal shear strength properties along the 2–3 and 3–1 planes, respectively, while S is the corresponding in-plane (1–2) shear strength property of the ply. All of the strength components are given from experimental tests, with the exception of F_{12} which is estimated using empirical methods that have proven satisfactory for composite materials [28].

The stress components $\sigma_j = (\sigma_j)_{elc}$ in (10) are the stresses of a candidate material c exerted on ply l of element e. The FE-version of the stresses are given in compact form as

$$\begin{aligned}\boldsymbol{\sigma}_{elc}(\tilde{\rho},\tilde{\mathbf{x}},\boldsymbol{\xi}) \quad &= \boldsymbol{D}_{elc}(\boldsymbol{\xi})\boldsymbol{u}(\tilde{\rho},\tilde{\mathbf{x}},\boldsymbol{\xi}) \\ &= \boldsymbol{T}_c^{-1}\boldsymbol{E}_c(\boldsymbol{\xi})\boldsymbol{B}_{el}\boldsymbol{L}_e^{\mathrm{T}}\boldsymbol{u}(\tilde{\rho},\tilde{\mathbf{x}},\boldsymbol{\xi})\end{aligned}, \quad \forall\,(e,l,c) \tag{12}$$

where $\boldsymbol{B}_{el}$ is the strain–displacement matrix of ply l, $\boldsymbol{L}_e$ selects the displacement components of element e from the global displacement vector $\boldsymbol{u}$. Note that in (10)–(12), the strength components F_j, F_{ij} and stresses σ_j are all expressed in the local M-frame of reference.

For an FE-discretized structure, the stresses $\boldsymbol{\sigma}_{elc}$ and therefore the failure index $\mathcal{F}_{elc}$, can be evaluated for any given number of sampling points for each ply l and element e. For a large number of sampling points, this can result in a high computational cost for the evaluation of the failure index. Therefore we only consider one sampling point, namely the centroid of each ply l in an element e when evaluating $\mathcal{F}_{elc}$.

4. Optimization problems

The present work intends to investigate the effects of material uncertainty on composite design for stiffness driven optimization problems. The investigation is done in two steps: first a design problem (DO) is solved using nominal values for constitutive properties, $(\tilde{\rho},\tilde{\mathbf{x}},\boldsymbol{\xi}^{\mathrm{N}})$, where $\boldsymbol{\xi}^{\mathrm{N}}$ represents a fixed value of the uncertainty variables such that the material properties correspond to their nominal values. In the second step, the design obtained in step one is fixed, $(\tilde{\rho}^*,\tilde{\mathbf{x}}^*,\boldsymbol{\xi})$ and a worst-case counterpart (WCC) problem is solved, for which a worst-case distribution of the material properties are determined and the impact on the objective function is evaluated. Fig. 1 shows the flowchart for the proposed method. Here the sub-solver depends on the optimization solver, for example in DO we apply GCMMA with IPOPT as a sub-solver, further described in Section 5.

The investigation will be performed for two types optimization metrics: compliance and strength using composite failure criteria, respectively. It is shown in Appendix B that, keeping the Poisson's ratio fixed, the worst case for the compliance is always the lowest allowable elastic modulii. Therefore the compliance problem should mainly be considered as a way to validate the proposed method for handling material uncertainty. Section 4.1 provides the design problem formulations for both optimization problems, while Section 4.2 provides the problem formulations for both worst-case counterparts of the design problems.

4.1. Design problem

In the design problem the objective is to minimize the compliance or a composite failure index of a composite laminate plate, respectively, under design and manufacturing constraints. The design problem for an objective function $f(\tilde{\rho},\tilde{\mathbf{x}},\boldsymbol{\xi}^{\mathrm{N}})$ is given by

$$\text{DO} \quad \begin{cases} \min_{\rho,\boldsymbol{x}} f(\tilde{\rho},\tilde{\mathbf{x}},\boldsymbol{\xi}^{\mathrm{N}}) \\ \text{s.t.} \begin{cases} \text{SE:} & \boldsymbol{K}(\tilde{\rho},\tilde{\mathbf{x}},\boldsymbol{\xi}^{\mathrm{N}})\boldsymbol{u}(\tilde{\rho},\tilde{\mathbf{x}},\boldsymbol{\xi}^{\mathrm{N}}) = \boldsymbol{F} & \\ \text{DC1:} & h_{\text{ply}} n_l \sum_{e=1}^{n^e} \tilde{\rho}_e a_e \leq V & \\ \text{MC1:} & -S \leq \tilde{\rho}_e n_l - \tilde{\rho}_j n_l \leq S & ,\forall\, i,j \in \mathbb{M}_e \\ \text{MC2:} & \sum_{l=t}^{t+n_{\text{CL}}} \tilde{x}_{plc} \leq n_{\text{CL}} & ,\forall\,(l,c) \\ \text{MC3:} & \sum_{l=1}^{n_l} \tilde{x}_{plc} \geq n_{\text{CML}} & ,\forall\,(p,c) \\ & \rho_e \in [0,1] & ,\forall\, e \\ & x_{el} \in [0,1] & ,\forall\,(e,l)\,. \end{cases} \end{cases}$$

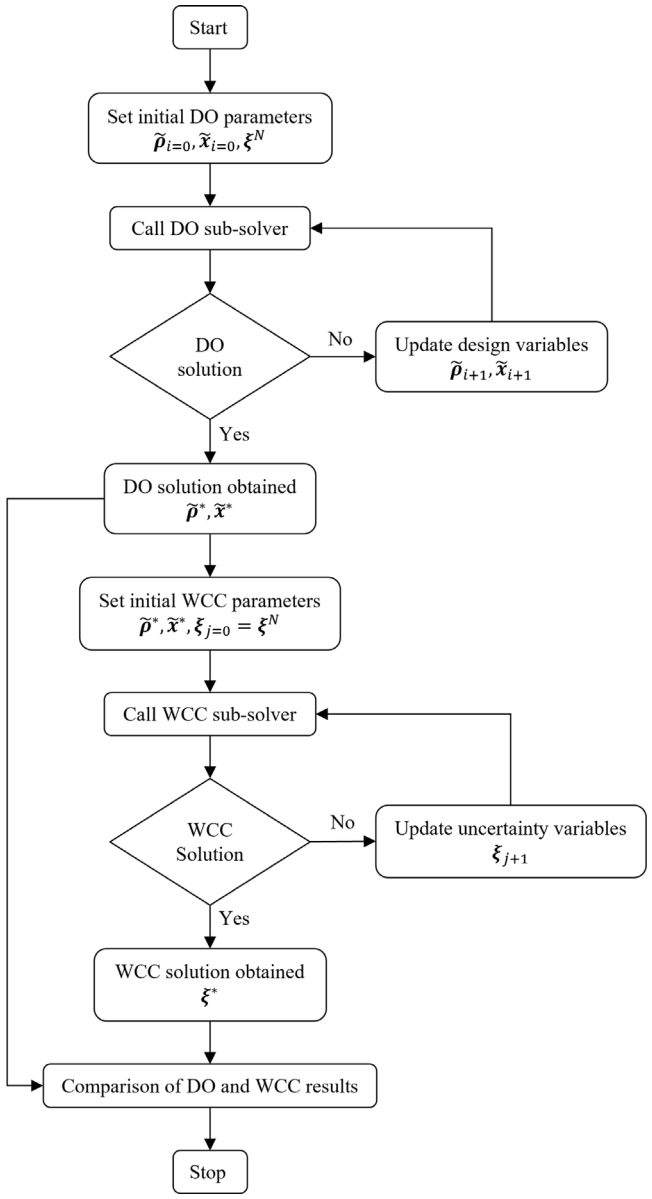

Fig. 1. Flowchart describing the optimization scheme for proposed method to evaluate the effects of material uncertainty on composite designs.

(13)

Here the state equation (SE) is taken to be a static linear elastic FE formulation in which $\boldsymbol{K}(\tilde{\rho}, \tilde{\boldsymbol{x}}, \xi^{\mathrm{N}})$ is the global stiffness matrix, $\boldsymbol{u}(\tilde{\rho}, \tilde{\boldsymbol{x}}, \xi^{\mathrm{N}})$ is the global displacement vector and $\boldsymbol{F}$ is the global load vector. Design constraint 1 (DC1), is a limit on the total amount of material to be distributed within the design domain and is set as a volume constraint where, a_e is the area of finite element e, h_{ply} is the ply thickness and V is the upper limit of the volume. Furthermore, three composite manufacturing constraints (MCs) are also included. MC1 is an explicit constraint on the thickness variation of the composite design which is set by limit S [32]. MC2 sets an upper limit on the number of consecutive plies (n_{CL}) that can have the same candidate material. MC3 provides the lower limit on the total number of plies (n_{CML}) of a given candidate material within the laminate.

The objective function $f(\tilde{\rho}, \tilde{\boldsymbol{x}}, \xi^{\mathrm{N}})$ in the respective design problems is defined in Sections 4.1.1 and 4.1.2.

4.1.1. Compliance problem

The objective function for the compliance version of (DO) is

$$f(\tilde{\rho}, \tilde{\boldsymbol{x}}, \xi^{\mathrm{N}}) = \boldsymbol{F}^{\mathrm{T}} \boldsymbol{u}(\tilde{\rho}, \tilde{\boldsymbol{x}}, \xi^{\mathrm{N}}) = \boldsymbol{u}(\tilde{\rho}, \tilde{\boldsymbol{x}}, \xi^{\mathrm{N}})^{\mathrm{T}} \boldsymbol{K}(\tilde{\rho}, \tilde{\boldsymbol{x}}, \xi^{\mathrm{N}}) \boldsymbol{u}(\tilde{\rho}, \tilde{\boldsymbol{x}}, \xi^{\mathrm{N}}), \quad (14)$$

where $\boldsymbol{u}(\tilde{\rho}, \tilde{\boldsymbol{x}}, \xi^{\mathrm{N}})$ solves the state equation SE in (13), and the global stiffness matrix is given by

$$\begin{aligned} \boldsymbol{K}(\tilde{\rho}, \tilde{\boldsymbol{x}}, \xi^{\mathrm{N}}) &= \sum_{p=1}^{n_p} \mathop{\mathbf{A}}_{e \in \mathcal{P}_p} \boldsymbol{K}_e(\tilde{\rho}, \tilde{\boldsymbol{x}}, \xi^{\mathrm{N}}) \\ &= \sum_{p=1}^{n_p} \mathop{\mathbf{A}}_{e \in \mathcal{P}_p} \sum_{l=1}^{n_l} \int_{\Omega_{el}} \boldsymbol{B}_e^{\mathrm{T}} \boldsymbol{E}_{el}(\tilde{\rho}, \tilde{\boldsymbol{x}}, \xi^{\mathrm{N}}) \boldsymbol{B}_e dV, \end{aligned} \quad (15)$$

in which $\mathbf{A}$ represents the FE assembly operator, $\boldsymbol{B}_e$ is the elemental strain–displacement matrix, see [33], and $\boldsymbol{E}_{el}$ is given by (1). Note that in (15), index $p = 1, \ldots, n_p$ refers to the division of the design domain into a number of sub-domains named patches. Each patch p is made up of a given number of finite element e, such that all elements in a patch retain the same properties. Patches can be defined independently to control any given property, such as density variables ρ or candidate material variables $\boldsymbol{x}$. For a detailed discussion on the use of patches the authors refer to [27,34].

4.1.2. Strength problem

The objective function for strength-based design to be used by (DO) is defined using the ℓ^p-norm. This enables all failure criteria indexes of the design domain to be included into a single smooth function [29]. The objective function is given as

$$f(\tilde{\rho}, \tilde{\boldsymbol{x}}, \xi^*) = \left\| \mathcal{F}\left(\boldsymbol{\sigma}(\tilde{\rho}, \tilde{\boldsymbol{x}}, \xi^{\mathrm{N}})\right) \right\|_P \quad (16)$$

where

$$\begin{aligned} \left\| \mathcal{F}\left(\boldsymbol{\sigma}(\tilde{\rho}, \tilde{\boldsymbol{x}}, \xi^{\mathrm{N}})\right) \right\|_P &= \left(\sum_{e=1}^{n_e} \sum_{l=1}^{n_l} \left| \mathcal{F}_{el}^{\mathrm{eff}}\left(\boldsymbol{\sigma}(\tilde{\rho}, \tilde{\boldsymbol{x}}, \xi^{\mathrm{N}})\right) \right|^P \right)^{1/P} \\ &= \left(\sum_{e=1}^{n_e} \sum_{l=1}^{n_l} \left| \sum_{c=1}^{n_c} \psi_{elc}(\tilde{\rho}, \tilde{\boldsymbol{x}}) \mathcal{F}_{elc}\left(\boldsymbol{\sigma}_{elc}(\tilde{\rho}, \tilde{\boldsymbol{x}}, \xi^{\mathrm{N}})\right) \right|^P \right)^{1/P}, \end{aligned} \quad (17)$$

Here $P > 1$ is a parameter such that as $\mathcal{F}\left(\boldsymbol{\sigma}(\tilde{\rho}, \tilde{\boldsymbol{x}}, \xi^{\mathrm{N}})\right) \to \mathcal{F}_{elc}^{\max}\left(\boldsymbol{\sigma}(\tilde{\rho}, \tilde{\boldsymbol{x}}, \xi^{\mathrm{N}})\right)$ as $P \to \infty$. In general when using the ℓ^p-norm, large values for P are desirable as it gives a better approximation of the max-function value, but this can lead to numerical difficulties when solving the optimization problem. Herein we follow [29] and use a fixed value of $P = 8$.

4.2. Worst-case problem

In this section the worst-case counterparts of the design problems in Section 4.1 are defined. For a fixed design $(\rho^*, \boldsymbol{x}^*)$ obtained from (DO) and a given structural response as a function of the uncertainty variables, i.e., $f(\xi) = f(\rho^*, \boldsymbol{x}^*, \xi)$, we consider finding the worst possible response over the uncertainty space $\mathcal{M}$, i.e. we solve

$$\max_{\xi \in \mathcal{M}} f(\xi),$$

where it is assumed that largest value of f corresponds to the worst performance. The worst-case counterpart of (DO) is stated as

$$\text{WCC} \quad \begin{cases} \max_{\xi \in \mathcal{M}} f(\xi) \\ \text{s.t.} \begin{cases} \text{SE:} \quad \boldsymbol{K}(\xi)\boldsymbol{u}(\xi) = \boldsymbol{F} \end{cases} \end{cases} \quad (18)$$

Compared to (DO), (WCC) only consider the effect of material uncertainty on the objective function $f(\xi)$. As the design is fixed in (WCC) the design and manufacturing constraints are not active and are excluded from the problem formulation. The objective function $f(\xi)$ in (WCC) is defined in Section 4.2.1 for the compliance problem and in Section 4.2.2 for the strength problem, respectively, along with their respective sensitivity data with respect to the uncertainty variables ξ.

4.2.1. Compliance problem

The objective function for compliance in (WCC) is given as

$$f(\xi) = \boldsymbol{u}(\xi)^{\mathsf{T}} \boldsymbol{K}(\xi) \boldsymbol{u}(\xi) \tag{19}$$

The sensitivity of the objective function in (19) is given by

$$\frac{\partial f(\xi)}{\partial \xi_n} = -\boldsymbol{u}(\xi)^T \frac{\partial \boldsymbol{K}(\xi)}{\partial \xi_n} \boldsymbol{u}(\xi), \quad \forall\, n, \tag{20}$$

where

$$\begin{aligned} \frac{\partial \boldsymbol{K}(\xi)}{\partial \xi_n} &= \sum_{e=1}^{n_e} \frac{\partial \boldsymbol{K}_e(\xi)}{\partial \xi_n} \\ &= \sum_{e=1}^{n_e} \sum_{l=1}^{n_l} \int_{\Omega_{el}} \boldsymbol{B}_e^{\mathsf{T}} \frac{\partial \boldsymbol{E}_{el}(\xi)}{\partial \xi_n} \boldsymbol{B}_e dV. \end{aligned} \tag{21}$$

Here, using (1) and (3),

$$\frac{\partial \boldsymbol{E}_{el}(\xi)}{\partial \xi_n} = v_{el} \sum_{c=1}^{n_c} \omega_{elc} \frac{\partial \boldsymbol{E}_c(\xi)}{\partial \xi_n}, \quad \forall\, (e,l) \tag{22a}$$

$$\frac{\partial \boldsymbol{E}_c(\xi)}{\partial \xi_n} = \boldsymbol{T}_c^{\mathsf{T}} \frac{\partial \boldsymbol{C}(\xi)}{\partial \xi_n} \boldsymbol{T}_c, \quad \forall\, c, \tag{22b}$$

where the derivatives of the constitutive matrix $\boldsymbol{C}(\xi)$ are given in Appendix A.

4.2.2. Strength problem

The objective function of (WCC) for the strength problem is given by (16)–(17), with only active uncertainty variables ξ:

$$f(\xi) = \left\| \mathcal{F}(\xi) \right\|_P \tag{23a}$$

$$\begin{aligned} \left\| \mathcal{F}(\xi) \right\|_P &= \left(\sum_{e=1}^{n_e} \sum_{l=1}^{n_l} \left| \mathcal{F}_{el}^{\text{eff}}(\boldsymbol{\sigma}(\xi)) \right|^P \right)^{1/P} \\ &= \left(\sum_{e=1}^{n_e} \sum_{l=1}^{n_l} \left| \sum_{c=1}^{n_c} \psi_{elc} \mathcal{F}_{elc}(\boldsymbol{\sigma}(\xi)) \right|^P \right)^{1/P}. \end{aligned} \tag{23b}$$

The sensitivity of the objective function in (23a) is given by

$$\frac{\partial f(\xi)}{\partial \xi_n} = \frac{\partial \left\| \mathcal{F}(\xi) \right\|_P}{\partial \xi_n}, \quad \forall\, n. \tag{24}$$

Using (23b) we get

$$\begin{aligned} \frac{\partial \left\| \mathcal{F}(\xi) \right\|_P}{\partial \xi_n} = \; & \left\| \mathcal{F}(\xi) \right\|_P^{\frac{1-P}{P}} \sum_{e=1}^{n_e} \sum_{l=1}^{n_l} \left| \mathcal{F}_{el}(\boldsymbol{\sigma}) \right|^{P-1} \\ & \sum_{c=1}^{n_c} \psi_{elc} \frac{\partial \mathcal{F}_{elc}^{\mathsf{T}}(\boldsymbol{\sigma})}{\partial \boldsymbol{\sigma}_{elc}} \frac{\partial \boldsymbol{D}_{elc}(\xi)}{\partial \xi_n} \boldsymbol{u}(\xi) - \lambda^{\mathsf{T}}(\xi) \frac{\partial \boldsymbol{K}(\xi)}{\partial \xi_n} \boldsymbol{u}(\xi), \end{aligned} \tag{25}$$

where $\frac{\partial \boldsymbol{K}(\xi)}{\partial \xi_n}$ is given by (21) and $\frac{\partial \mathcal{F}_{elc}(\boldsymbol{\sigma})}{\partial \boldsymbol{\sigma}_{elc}}$ is expressed using (10) as

$$\frac{\partial \mathcal{F}_{elc}(\boldsymbol{\sigma})}{\partial \boldsymbol{\sigma}_{elc}} = \begin{pmatrix} F_1 + 2F_{11}\sigma_1 + 2F_{12}\sigma_2 \\ F_2 + 2F_{22}\sigma_2 + 2F_{12}\sigma_1 \\ 2F_{44}\sigma_4 \\ 2F_{55}\sigma_5 \\ 2F_{66}\sigma_6 \end{pmatrix}, \quad \forall\, (e,l,c). \tag{26}$$

From (12), $\frac{\partial \boldsymbol{D}_{elc}(\xi)}{\partial \xi_n}$ in (25) is given as

$$\frac{\partial \boldsymbol{D}_{elc}(\xi)}{\partial \xi_n} = \boldsymbol{T}_c^{-1} \frac{\partial \boldsymbol{E}_c(\xi)}{\partial \xi_n} \boldsymbol{B}_{el} \boldsymbol{L}_e^{\mathsf{T}}, \tag{27}$$

where $\frac{\partial \boldsymbol{E}_c(\xi)}{\partial \xi_n}$ is given by (22). The adjoint vector λ in (25) is obtained by solving the adjoint equation

$$\boldsymbol{K}(\xi)\, \lambda(\xi) = \boldsymbol{\Lambda}^{\mathsf{T}}(\xi)$$

in which

$$\boldsymbol{\Lambda}(\xi) = \left\| \mathcal{F}(\xi) \right\|_P^{\frac{1-P}{P}} \sum_{e=1}^{n_e} \sum_{l=1}^{n_l} \left| \mathcal{F}_{el}(\boldsymbol{\sigma}) \right|^{P-1} \sum_{c=1}^{n_c} \psi_{elc} \frac{\partial \mathcal{F}_{elc}^{\mathsf{T}}(\boldsymbol{\sigma})}{\partial \boldsymbol{\sigma}_{elc}} \boldsymbol{D}_{elc}(\xi). \tag{28}$$

Table 1
Nominal values for material data of HTA7/6376 CFRP-UD.

Property		Value	Unit
Longitudinal modulus	E_1	141	GPa
Transverse modulus	E_2	10	GPa
In-plane shear modulus	G_{12}	5.2	GPa
Transverse shear modulus	G_{23}	3.9	GPa
Transverse shear modulus	G_{13}	5.2	GPa
In-plane Poisson's ratio	ν_{12}	0.3	–
Longitudinal tensile strength	X_t	2250	MPa
Longitudinal compressive strength	X_c	1400	MPa
Transverse tensile strength	Y_t	65	MPa
Transverse compressive strength	Y_c	300	MPa
In-plane shear strength	S	120	MPa
Transverse shear strength	R	80	MPa
Transverse shear strength	Q	80	MPa
Cured ply thickness	h_{ply}	$1.3 \cdot 10^{-4}$	m

Table 2
Initial values for design and uncertainty variables.

Property		Value	
Density variables	ρ_e^{init}	0.50	$\forall\, e$
Candidate material variables	x_{el}^{init}	0.50	$\forall\, (e,l)$
Material uncertainty variables	ξ_n^{init}	1.00	$\forall\, n$

Table 3
Filter and penalization parameter sets for HFP.

Property	Set	Numerical value
Candidate material filter	$\mathbb{N}_\alpha$	20, 40, 60, 80, 160, 320
Candidate material penalization	$\mathbb{N}_p$	2
Ply density filter	$\mathbb{N}_\beta$	13, 40, 80, 180
Ply density penalization	$\mathbb{N}_q$	0, 2, 4
Strength penalization	$\mathbb{N}_r$	0, -0.4, -0.8

Table 4
Convergence tolerances for the optimization algorithm.

Property		DO	WCC
Non-discreteness tolerance	$\epsilon_{0/1}$	0.1%	–
Design variable tolerance	ϵ_{dv}	10^{-3}	10^{-6}
Objective function tolerance	ϵ_{obj}	10^{-6}	10^{-6}
Constraint functions tolerance	ϵ_{const}	10^{-6}	10^{-6}

5. Numerical examples

This section describes the numerical examples used to evaluate the effects of material uncertainty on stiffness driven design problem for composite laminate structures. Three designs are obtained by solving (DO) and then analyzed by solving (WCC) to find the worst-case deviation of the material properties from their nominal values. The examples are based on two geometries that are subjected to various boundary conditions and loads. The material data used correspond to a unidirectional Carbon Fiber Reinforced (CFRP-UD) material, HTA7/6376 [35] with nominal values listed in Table 1. A set of $n_c = 4$ candidate materials are used for all numerical examples. Each candidate $c = 1, \ldots, n_c$ represents a fiber orientation of the UD-ply from the set {0°, 45°, -45°, 90°}. The starting values of the design variables used for the optimization runs is given in Table 2.

Table 3 shows the sets of filter and penalization parameters used by the optimization algorithm to solve the numerical examples. The convergence tolerances for the optimization algorithm are given in Table 4.

The FE discretization is done using 9-noded iso-parametric, fully integrated second-order elements with five degrees-of-freedom per node, based on the Mindlin–Reissner plate element formulation; see for example [33,36].

For DO, all numerical examples are solved using a modified version of the Globally Convergent Methods of Moving Asymptotes (GCMMA)

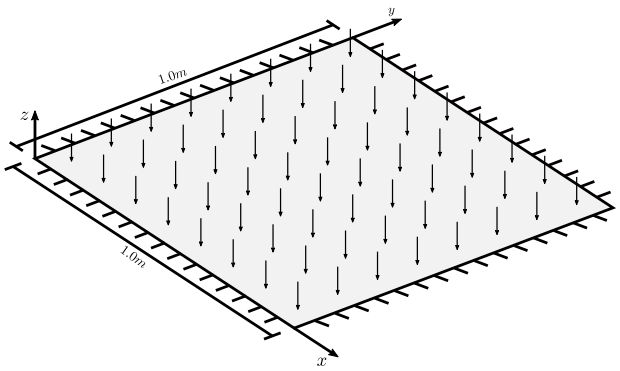

Fig. 2. NE1 geometry and boundary conditions. Clamped square plate with edge length of 1.0 m, subjected to a uniform pressure $q = 3.0$ kPa.

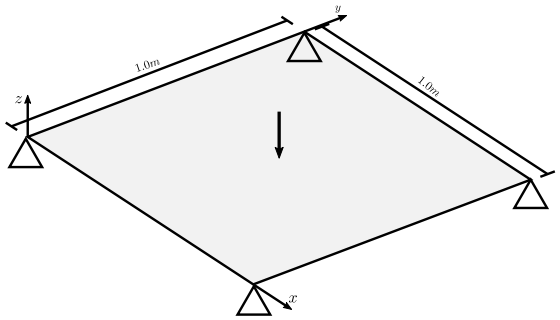

Fig. 3. NE2 geometry and boundary conditions. Corner hinged square plate with edge length of 1.0 m, subjected to a concentrated force of $F = 500$ N applied at the midpoint.

solver [37,38] described in [27]. The GCMMA sub-problem is solved using IPOPT [39] as sub-solver which treats the constraints using an interior-point methods [40]. The solution of (WCC) was tested using a number of different optimization solvers: the genetic algorithm from the MATLAB Global Optimization Toolbox (GA), GCMMA using both IPOPT and the default sub-solver based on an interior point algorithm, and FMINCON using the interior-point and active-set algorithms [41]. While all tested methods gave the same solution, it was found in all cases that FMINCON using the active-set algorithm performed superior in terms of number of function evaluations and CPU time, with a solution time on the order of a few seconds.

5.1. Geometry and boundary conditions

This section gives a short description of the set-up for the numerical examples (NE). In terms of geometry and boundary conditions NE1 and NE3 are taken to be the same as presented in [27] while NE2 is given in [29].

Fig. 2 illustrates the set-up for NE1, a square composite laminate plate with clamped edges subjected to a uniform pressure load $q = 3.0$ kPa across the top surface.

Fig. 3 illustrates the set-up for NE2. Here a corner hinged square composite laminate plate is shown that is subjected to a concentrated load $F = 500$ N at the midpoint of the top surface.

The set-up of NE3 is illustrated in Fig. 4, which shows a cantilever rectangular composite laminate plate with an out-of-plane torque load applied at the free edge such that the plate is subjected to a torsion load case. The magnitude of the torque load is set to $M_\tau = 30$ Nm.

The numerical examples all consider a monolithic composite laminate with a maximum of sixteen plies, $n_l = 16$, which corresponds to a maximum total laminate thickness of 2.08 mm. A single design patch, $n_p = 1$, is used across the design domain for the candidate material

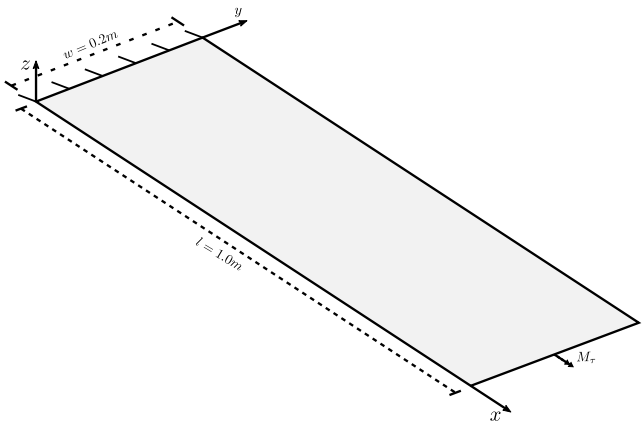

Fig. 4. NE3 geometry and boundary conditions. A rectangular cantilever plate with length $l = 1$ m and width $w = 0.2$ m, subjected to an out-of-plane torque load of $M_\tau = 30$ Nm at the free edge.

Table 5
Optimization settings for the numerical examples.

	Design problem			Worst-case problem		
ID	NE1.01	NE2.01	NE3.01	NE1.02	NE2.02	NE3.02
n_e	400	400	500	400	400	500
n_l	16	16	16	16	16	16
n_c	4	4	4	4	4	4
n_p	1	1	1	1	1	1
n_{S}	1	1	1	-	-	-
n_{CL}	1	1	1	-	-	-
n_{CML}	2	2	0	-	-	-
V/V_0	0.5	0.5	0.5	-	-	-
$\underline{\rho_e}$	1/16	1/16	1/16	-	-	-
$\underline{\xi_n}\backslash\overline{\xi_n}$	-	-	-	0.9\1.1	0.9\1.1	0.9\1.1

design variables $\boldsymbol{x}$ in (DO), thus providing a global lay-up sequence for the entire domain. No patches were used on the density variables $\boldsymbol{\rho}$ in (DO), thus allowing for unrestricted distribution of composite material within the design domain. All laminates are required to have one full ply throughout the design domain. This is achieved by setting the lower bound of the density variable ρ_e in (13) to $\underline{\rho_e} = 1/n_l$. For the design and manufacturing constraints used in (DO), the following limits have been used. For DC1, an upper limit of the volume, $V/V_0 = 0.5$ is set for the whole design domain, thus only half the available material is used. The limit of MC1 is set to $n_{\mathrm{S}} = 1$ for the maximum ply thickness variation between adjacent elements. The same limit is set for MC2, $n_{\mathrm{CL}} = 1$, which restricts the number of consecutive plies with a given candidate material. For MC3, the limit is set to $n_{\mathrm{CML}} = 2$ for NE1 and NE2, that require a minimum of 10% of each candidate material to be used in the design. For NE3, the limit is set to $n_{\mathrm{CML}} = 0$ which does not put any lower limit to the minimum amount of each candidate material. The bounds of all uncertainty variables ξ_n in (WCC) are assumed to be equal and set to $\underline{\xi_n} = 0.9$ and $\overline{\xi_n} = 1.1$ for all NE. These bounds represent a 10% deviation of the independent material properties from their nominal values in Table 1, so that for example, $9\,\mathrm{GPa} \leq E_2 \leq 11\,\mathrm{GPa}$. A summary of all optimization settings for the numerical examples is given in Table 5.

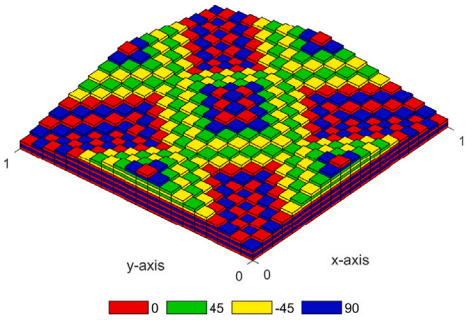

(a) NE1.01, Design given by (DO).

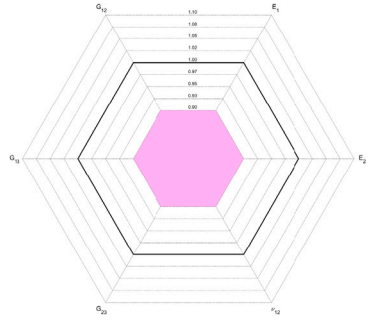

(b) NE1.02, Deviation of material properties from nominal values given by (WCC).

Fig. 5. NE1 — Results from (DO) and (WCC) for the compliance problem.

6. Results

In this section we present the results for the three numerical examples described in Section 5 and a short discussion is given regarding the generated data. Section 6.1 presents the results for the compliance problem as described in Sections 4.1.1 and 4.2.1. The results for the strength-based problem described in Sections 4.1.2 and 4.2.2 are presented in Section 6.2.

6.1. Compliance problem

For the compliance optimization problem all numerical runs retain a high level of non-discreteness for the design variables. The results obtained for NE1, 2, and 3 are visualized in Fig. 5, Fig. 6 and Fig. 7 respectively. The effects of material uncertainty on the compliance is presented in Table 6.

Fig. 5(a) shows the composite design given by (DO) for NE1 using nominal material properties. The composite laminate contains predominantly 0°/90° plies with minimum amount of off-axis ±45° plies and the material distribution across the design domain is symmetric. Fig. 5(b) shows the worst-case deviation of the independent material properties obtained from (WCC) for the design in Fig. 5(a). In the spider diagram in Fig. 5(b) the solid black line represents the nominal values and each axis corresponds to a material parameter, where change in values is along respective axis. The worst-case values for all material properties coincides with the lower bound of the uncertainty variables which represents a 10% decrease of the material properties. Although a global optimum is not guaranteed by solving (WCC), for simplicity these values are henceforth refereed to as worst-case values.

For NE2, Fig. 6(a) shows the composite design given by (DO) with nominal material properties. The material distribution is symmetric and the laminate contain predominantly off-axis ±45° plies while the amount of 0°/90° is at the lower limit set by the MC1 constraint, $n_{\mathrm{CML}} = 2$, in (DO). Fig. 6(b) shows that the worst-case deviation of the material properties for NE2 is at the lower limit for all uncertainty variables and corresponds to a 10% decrease of the constitutive properties.

Fig. 7 shows the results for NE3. The composite laminate in Fig. 7(a) contains only off-axis ±45° plies and is a valid solution as MC1 in (DO) is set to $n_{\mathrm{CML}} = 0$ for this example. Fig. 7(b) shows that NE3 follows a similar pattern to NE1 and NE2 for (WCC) in that, with the exception of ν_{12}, the independent material properties retain a value of the uncertainty variables at the lower limit with an overall decrease of 10% value of material properties. For ν_{12}, Fig. 7(b) indicate that the worst-case value is at the upper limit of the associated uncertainty variable.

Table 6
Effect of material uncertainty on the compliance. f is the objective function value, and Δf is difference between objective function value from (DO) and (WCC).

Run ID	Problem	f	Δf
NE1.01	DO	401.44	11.4%
NE1.02	WCC	447.29	
NE2.01	DO	919.73	11.4%
NE2.02	WCC	1024.34	
NE3.01	DO	111.82	11.4%
NE3.02	WCC	124.57	

Table 6 summarizes the effects of material uncertainty on the compliance for all NE:s. The results presented in Table 6 show that the compliance increases with 11.4% for WCC compared to DO with nominal material properties. This is observed for all numerical examples and correlates well to the decrease of 10% of the material properties that was observed for WCC results in Figs. 5–7. The result for NE3 in Fig. 7 and Table 6 indicate that the Poisson's ratio ν_{12} does not have an significant impact on material uncertainty as Δf for NE3 is the same as for NE1 and NE2, respectively. The results for the compliance case verify the conclusions provided in Appendix B that worst-case results correspond to the elastic moduli attaining their respective lower bound.

6.2. Strength-based problem

For the strength-based optimization problem the results generated by (DO) and (WCC) for NE1 are visualized in Fig. 8 while Figs. 9 and 10 shows the results for NE2 and NE3, respectively. All designs obtained by (DO) have a high level of non-discreteness of the design variable. The effect of material uncertainty on the objective of the optimization problem is given in Table 7.

Fig. 8(a) shows the composite design provided by (DO) using nominal material properties. We observe a symmetric material distribution and the composite laminate contains an even mixture of both 0°/90° and off-axis ±45° plies. The spider diagram in Fig. 8(b) shows the worst-case deviation of the nominal properties from their nominal values obtained by (WCC). Here the worst-case deviation correspond to E_2 and ν_{12} at the upper bound of the uncertainty variables while the remaining material properties are at the lower bound. Figs. 8(c) and 8(d) show the maximum value of the effective failure index (8) across the design domain for (DO) and (WCC), respectively. The failure plots are scaled to their respective maximum value and a comparison indicate no change in the overall pattern of the failure index between (DO) and (WCC).

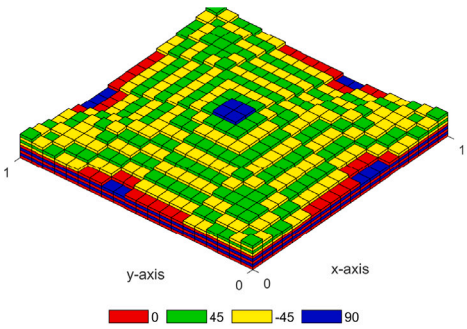

(a) NE2.01, Design given by (DO).

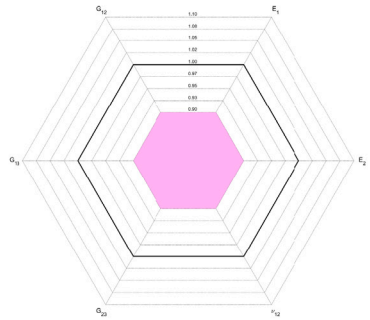

(b) NE2.02, Deviation of material properties from nominal values given by (WCC).

Fig. 6. NE2 — Results from (DO) and (WCC) for the compliance problem.

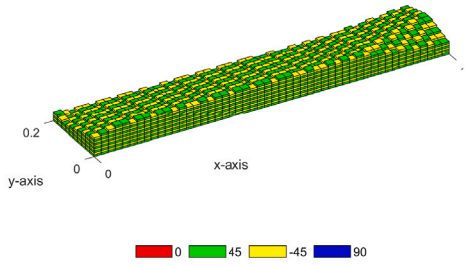

(a) NE3.01, Design given by (DO).

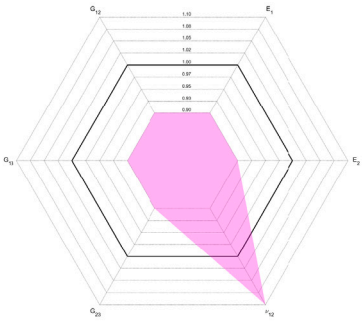

(b) NE3.01, Deviation of material properties from nominal values given by (WCC).

Fig. 7. NE3 — Results from (DO) and (WCC) for the compliance problem.

For NE2, Fig. 9(a) shows a composite laminate containing primarily off-axis ±45° plies with a minimum amount of 0°/90°, and a symmetric material distribution. Fig. 9(b) presents a worst-case deviation of the material properties for NE2 in which E_1 and ν_{12} take on values at the lower limit of the uncertainty variables while the remaining independent material properties are set to the upper limit. The failure index plots displayed in Figs. 9(c) and 9(d) follow the same pattern as the failure plots for NE1 in Fig. 8 which show no significant change in composite failure between (DO) and (WCC).

Fig. 10(a) shows the composite design given by (DO) for NE3. Much like design obtained in Fig. 7(a) for compliance, the composite laminate contains only off-axis ±45° plies. However, compared to the design in Fig. 7(a) the material distribution in Fig. 10(a) is of uniform thickness across the design domain for the strength based optimization problem. Furthermore, Fig. 10(b) displays the worst-case deviation, which for NE3 corresponds to values at the lower bound for E_1, G_{23} and ν_{12} while E_2, G_{12} and G_{13} retain values at the upper bound. As was the case for NE1 and NE2 in Fig. 8 and Fig. 9 respectively, Figs. 10(c) and 10(d) indicate no significant difference in composite failure between (DO) and (WCC) for NE3.

Table 7 shows the effect of material uncertainty on the objective of the strength-based optimization problem using Tsai–Wu failure criteria. Here f are the objective function values given by the ℓ^p-norm formulation in (17), while $\mathcal{F}_{el}^{\text{eff}}$ represent the maximum failure index (8) computed for the design. These results indicate that the ℓ^p-norm with $P = 8$ will, depending on the NE, overestimate the true maximum failure index of the designs with 27% – 34% compared to $\mathcal{F}_{el}^{\text{eff}}$. The overestimation of the ℓ^p-norm is consistent for (DO) and (WCC) for each NE, however further investigation is needed to improve the accuracy. The data in Table 7 shows an increase in the objective function value of 21.3% for NE1 when comparing (DO) and (WCC), and slightly higher difference of 23.7% for $\mathcal{F}_{el}^{\text{eff}}$ indices is observed. Similar effect is also present for NE2 where the objective function value increases with 22.8% and $\mathcal{F}_{el}^{\text{eff}}$ with 24.5% for WCC compared to DO. For NE3 we observe a lower impact of material uncertainty compared to NE1 and NE2 as the objective function increases with 17.8% and $\mathcal{F}_{el}^{\text{eff}}$ with 18.4%, respectively. Overall, for all three NE:s the data in Table 7 shows a significant impact of material uncertainty on the objective function and failure indexes for the designs, which for all numerical examples exceeds the ±10% change of the constitutive properties.

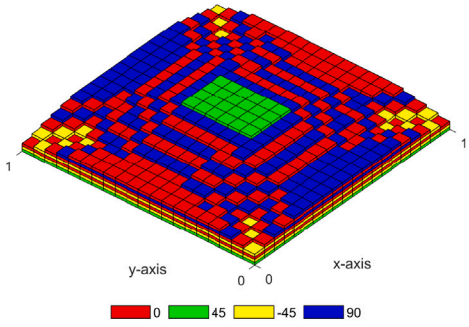

(a) NE1.01, Design given by (DO).

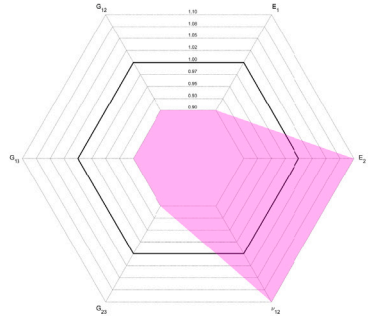

(b) NE1.02, Deviation of material properties from nominal values given by (WCC).

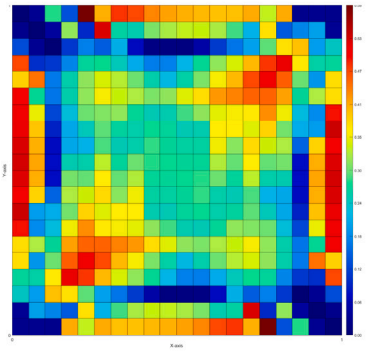

(c) NE1.01, Failure index (DO), where $\mathcal{F}^{\text{eff}}_{\max} = 0.59$

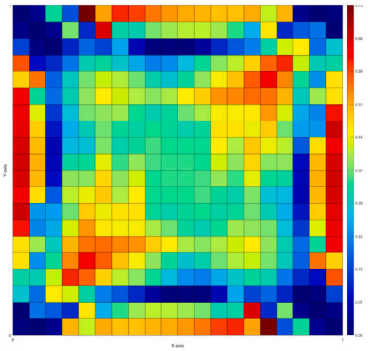

(d) NE1.02, Failure index (WCC), where $\mathcal{F}^{\text{eff}}_{\max} = 0.73$

Fig. 8. NE1 — Results from (DO) and (WCC) for the strength-based problem.

Table 7
Strength-based problem, effects of material uncertainty. f is the objective function value and $\mathcal{F}^{\text{eff}}_{el}$ is the maximum failure index. Δf and $\Delta\mathcal{F}^{\text{eff}}_{el}$ is the difference in objective function value and failure index, respectively, between DO and WCC.

Run ID	Problem	f	Δf	$\mathcal{F}^{\text{eff}}_{el}$	$\Delta\mathcal{F}^{\text{eff}}_{el}$
NE1.01	DO	0.89	21.3%	0.59	23.7%
NE1.02	WCC	1.08		0.73	
NE2.01	DO	1.36	22.8%	0.98	24.5%
NE2.02	WCC	1.67		1.22	
NE2.01	DO	0.90	17.8%	0.65	18.4%
NE2.02	WCC	1.06		0.77	

7. Conclusions

We have proposed a method to quantify the effects of material uncertainty on the response of composite laminate structures optimized using a simultaneous topology and material optimization approach for stiffness and strength-based problems. The method is based on the parametrization of independent constitutive properties of a composite material using a set of uncertainty variables that enable a direct coupling of the material properties to the composite design problem, and provides an efficient way to handle variations of material properties in stiffness driven design optimization problems. The method was evaluated on compliance and strength based optimization problems including different loads, boundary conditions and composite design- and manufacturing constraints. For the compliance problem, the results in Section 6 verifies the theoretical assumption in Appendix B when considering material uncertainty. It shows that the objective value increases in proportion to the decrease of the material properties for all numerical examples and the worst-case deviation coincide with the lower bound for the elastic moduli. For the strength-based problem, the results in Section 6 indicate that material uncertainty has a high impact on the failure of composite design. The results show an increase of 18% – 25% in failure index for the numerical examples when worst-case deviation of the material properties is considered. The deviation of material properties from their nominal values is not consistent, as each NE retains a unique combination of worst-case values for the independent material properties.

Uncertainty quantification with the proposed method provides an efficient approach to quantify the influence of material uncertainty on structural performance. The general formulation of WCC makes it directly applicable to all composite parametrization techniques for structural optimization. The limited size of the WCC optimization problem and the small number of function evaluations required, makes the proposed method suitable for integration in robust and reliability base structural optimization frameworks.

The proposed method was tested on designs optimized for either compliance or strength, but is readily applied to problem formulations were these responses are treated simultaneously, for example by combining them in a weighted sum or using one as objective and the other as constraint. As illustrated by the numerical examples, the UQ then has to be performed separately for each response as the worst material parameters for compliance may not be the same as those for strength.

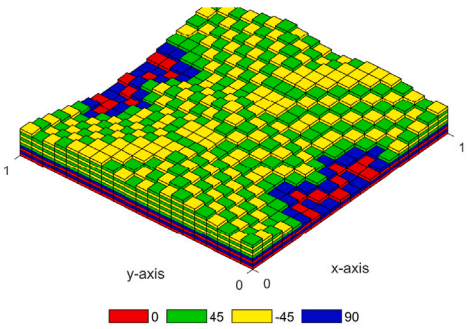

(a) NE2.01, Design given by (DO).

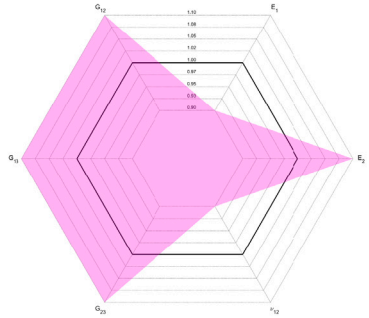

(b) NE2.02, Deviation of material properties from nominal values given by (WCC).

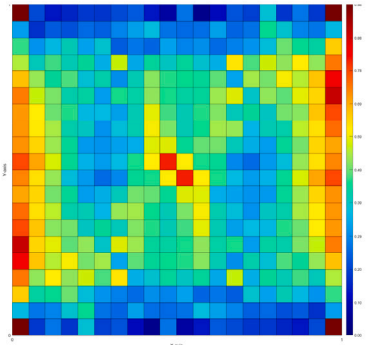

(c) NE2.01, Failure index (DO), where $\mathcal{F}^{\text{eff}}_{\max} = 0.98$

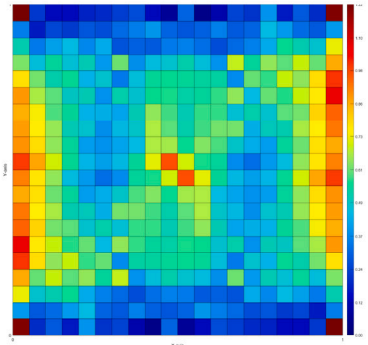

(d) NE2.02, Failure index (WCC), where $\mathcal{F}^{\text{eff}}_{\max} = 1.22$

Fig. 9. NE2 — Results from (DO) and (WCC) for the compliance problem.

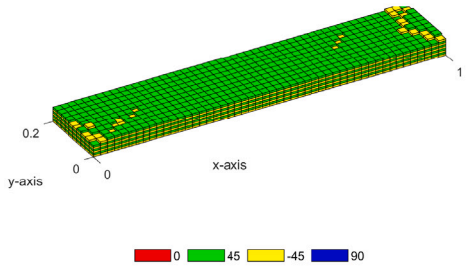

(a) NE3.01, Design given by (DO).

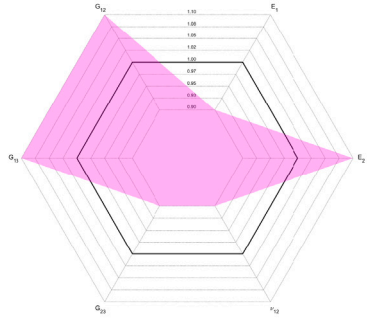

(b) NE3.02, Deviation of material properties from nominal values given by (WCC).

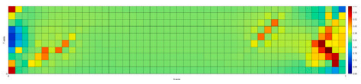

(c) NE3.01, Failure index (DO), where $\mathcal{F}^{\text{eff}}_{\max} = 0.65$

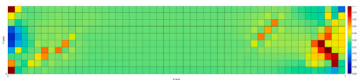

(d) NE3.02, Failure index (WCC), where $\mathcal{F}^{\text{eff}}_{\max} = 0.77$

Fig. 10. NE3 — Results from (DO) and (WCC) for the compliance problem.

CRediT authorship contribution statement

Dženan Hozić: Writing – original draft, Writing – review & editing, Conceptualization, Methodology, Software, Validation, Investigation, Data curation, Visualization. **Carl-Johan Thore:** Supervision, Writing – original draft, Writing – review & editing, Conceptualization, Methodology, Software, Validation. **Christopher Cameron:** Supervision, Writing – review & editing. **Mohamed Loukil:** Supervision, Writing – review & editing.

Declaration of competing interest

The authors declare that they have no known competing financial interests or personal relationships that could have appeared to influence the work reported in this paper.

Data availability

Data will be made available on request.

Acknowledgments

This work is financed by the Swedish Energy Agency (Energimyndigheten) through grant number P48175-1 and the Swedish Research Council under grant agreement No 2019–04615, and is associated with the Swedish Electromobility Center[1] (SEC). Their support is gratefully acknowledged. The authors would also like to thank Krister Svanberg for providing his implementation of GCMMA.

Appendix A. Derivatives of the constitutive matrix $C(\xi)$

The derivatives of the constitutive matrix $\boldsymbol{C}(\xi)$ in (22b) are given using (5)–(7) for all uncertainty variables ξ as given in Box I.

Appendix B. Worst case for the compliance problem

The compliance can be written in terms of the potential energy as[2]

$$\frac{1}{2}\boldsymbol{F}^{\mathsf{T}}\boldsymbol{u}(\boldsymbol{C}) = -\min_{\boldsymbol{v}\in\mathbb{R}^n}\left\{\frac{1}{2}\boldsymbol{v}^{\mathsf{T}}\boldsymbol{K}(\boldsymbol{C})\boldsymbol{v} - \boldsymbol{F}^{\mathsf{T}}\boldsymbol{v}\right\}, \tag{B.1}$$

where n is the number of degrees of freedom. Consider two constitutive matrices $\boldsymbol{C}_1$ and $\boldsymbol{C}_2$ such that $\boldsymbol{C}_2 \succ \boldsymbol{C}_1 \succ \boldsymbol{0}$ everywhere in the design domain (the notation $\boldsymbol{A} \succ \boldsymbol{B}$ means that $\boldsymbol{A} - \boldsymbol{B}$ is positive definite). We now show that

$$\frac{1}{2}\boldsymbol{F}^{\mathsf{T}}\boldsymbol{u}(\boldsymbol{C}_2) < \frac{1}{2}\boldsymbol{F}^{\mathsf{T}}\boldsymbol{u}(\boldsymbol{C}_1), \tag{B.2}$$

i.e. the matrix $\boldsymbol{C}_1$ gives a less stiff material (recall that compliance is inversely related to stiffness).

A stiffness matrix of the form

$$\boldsymbol{K}(\boldsymbol{C}) = \sum_{e=1}^{m}\int_{\Omega_e}\boldsymbol{B}_e^{\mathsf{T}}\boldsymbol{C}\boldsymbol{B}_e\,\mathrm{d}V$$

will be positive definite with appropriate support conditions and a positive definite constitutive matrix $\boldsymbol{C}$. Letting $\boldsymbol{v}$ be an arbitrary vector we get, since $\boldsymbol{C}_2 - \boldsymbol{C}_1 \succ \boldsymbol{0}$,

$$\boldsymbol{v}^{\mathsf{T}}\boldsymbol{K}(\boldsymbol{C}_2)\boldsymbol{v} - \boldsymbol{v}^{\mathsf{T}}\boldsymbol{K}(\boldsymbol{C}_1)\boldsymbol{v} = \boldsymbol{v}^{\mathsf{T}}\boldsymbol{K}(\boldsymbol{C}_2 - \boldsymbol{C}_1)\boldsymbol{v} > 0, \tag{B.3}$$

i.e. $\boldsymbol{v}^{\mathsf{T}}\boldsymbol{K}(\boldsymbol{C}_2)\boldsymbol{v} - \boldsymbol{v}^{\mathsf{T}}\boldsymbol{K}(\boldsymbol{C}_1)\boldsymbol{v}$. Using (B.1) we then get

$$\frac{1}{2}\boldsymbol{F}^{\mathsf{T}}\boldsymbol{u}(\boldsymbol{C}_2) = -\min_{\boldsymbol{v}\in\mathbb{R}^n}\left\{\frac{1}{2}\boldsymbol{v}^{\mathsf{T}}\boldsymbol{K}(\boldsymbol{C}_2)\boldsymbol{v} - \boldsymbol{F}^{\mathsf{T}}\boldsymbol{v}\right\} <$$
$$-\min_{\boldsymbol{v}\in\mathbb{R}^n}\left\{\frac{1}{2}\boldsymbol{v}^{\mathsf{T}}\boldsymbol{K}(\boldsymbol{C}_1)\boldsymbol{v} - \boldsymbol{F}^{\mathsf{T}}\boldsymbol{v}\right\} = \frac{1}{2}\boldsymbol{F}^{\mathsf{T}}\boldsymbol{u}(\boldsymbol{C}_1),$$

since (B.3) holds for arbitrary $\boldsymbol{v} \neq \boldsymbol{0}$. The compliance is thus monotone decreasing (with respect to the ordering defined by $\succeq$) in the constitutive matrix.

Now consider the worst-case problem

$$\max_{\boldsymbol{C}:\underline{\boldsymbol{C}}\preceq\boldsymbol{C}\preceq\overline{\boldsymbol{C}}}\frac{1}{2}\boldsymbol{f}^{\mathsf{T}}\boldsymbol{u}(\boldsymbol{C}),$$

with limits $\underline{\boldsymbol{C}}$ and $\overline{\boldsymbol{C}}$ on the constitutive matrix. We now show that the solution, i.e. the worst constitutive matrix is the lower limit $\underline{\boldsymbol{C}}$. To this end we use proof by contradiction. Assume that $\boldsymbol{C}^*$ is an optimal solution such that $\boldsymbol{C}^* \prec \underline{\boldsymbol{C}}$. By definition of an optimal solution we have

$$\frac{1}{2}\boldsymbol{f}^{\mathsf{T}}\boldsymbol{u}(\boldsymbol{C}^*) \geq \frac{1}{2}\boldsymbol{f}^{\mathsf{T}}\boldsymbol{u}(\boldsymbol{C}), \quad \forall \boldsymbol{C} : \underline{\boldsymbol{C}} \preceq \boldsymbol{C} \preceq \overline{\boldsymbol{C}}.$$

However, since $\boldsymbol{C}^* \prec \underline{\boldsymbol{C}}$ we also have

$$\frac{1}{2}\boldsymbol{f}^{\mathsf{T}}\boldsymbol{u}(\boldsymbol{C}^*) < \frac{1}{2}\boldsymbol{f}^{\mathsf{T}}\boldsymbol{u}(\underline{\boldsymbol{C}}). \tag{B.4}$$

Since $\underline{\boldsymbol{C}}$ is feasible, this contradicts the statement that $\boldsymbol{C}^*$ is an optimal solution such that $\boldsymbol{C}^* \prec \underline{\boldsymbol{C}}$. Therefore we must have $\boldsymbol{C}^* = \underline{\boldsymbol{C}}$. In other words, the "lowest" value of the constitutive matrix is the worst.

Keeping the Poisson's ratios in the constitutive matrix (5) fixed, this matrix is linear in $\xi = (\xi_1, \dots \xi_5)^{\mathsf{T}}$. Then the element-wise strict inequality $\xi_2 > \xi_1 > \boldsymbol{0}$ implies $\boldsymbol{C}(\xi_2) = \boldsymbol{C}(\xi_2 - \xi_1 + \xi_1) = \boldsymbol{C}(\xi_1) + \boldsymbol{C}(\xi_2 - \xi_1) \succ \boldsymbol{C}(\xi_1)$, whence it follows using a similar line of reasoning as in the previous paragraph that the "lowest" vector ξ_1 will be the worst.

Allowing for variations of the Poisson's ratio complicates the situation as seen next.

Poisson's ratio

While the problem of finding the worst constitutive matrix is trivially solvable if only the elastic moduli varies, finding the worst Poisson's ratio appears to be a more complex problem. To see this, consider the even simpler case of an isotropic material with fixed Young's modulus. With compliance as the response of interest, the problem of finding the worst Poisson's ratio reads:

$$\max_{\nu:\underline{\nu}\leq\nu\leq\overline{\nu}}\frac{1}{2}\boldsymbol{F}^{\mathsf{T}}\boldsymbol{u}(\nu).$$

Unlike for the Young's modulus, the compliance is not monotone in the Poisson's ratio. Nor is the compliance strictly convex in ν, in which case the solution would always be either $\nu = \underline{\nu}$ or $\nu = \overline{\nu}$. In general, the dependence on ν seems to be dependent on the boundary conditions. This is illustrated in Fig. B.11 which shows the compliance as a function of Poisson's ratio for a structure modeled as a single constant strain triangle (CST) membrane element for 2D elasticity (most materials have a Poisson's ratio in the interval $(0, 0.5)$, hence we have chosen the values as limits here).

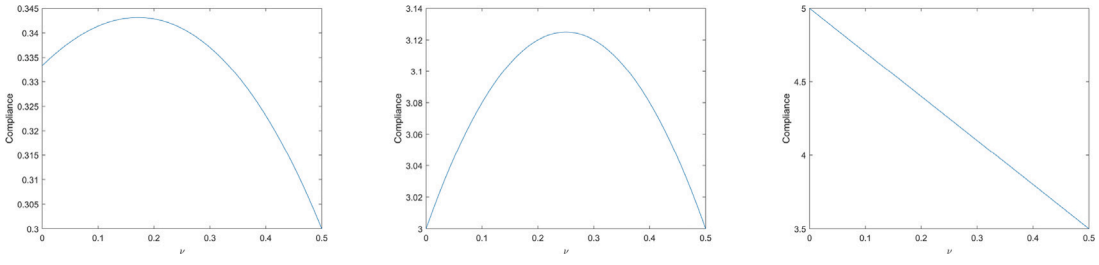

Fig. B.11. Compliance as a function of Poisson's ratio for a single CST element in plane stress with various DOFs locked. With $\overline{\nu} = 0$ and $\overline{\nu}$ and a load of the form $\boldsymbol{f} = \boldsymbol{1}$ we see that only in the right-most case (with solution $\nu = 0$) is the worst Poisson's ratio found at the boundary of the feasible set.

[1] SEC - https://emobilitycentre.se/.

[2] This is easy to verify by noting that a solution to the minimization problem must satisfy $\boldsymbol{K}(\boldsymbol{C})\boldsymbol{u} = \boldsymbol{F}$ and inserting this into the objective function.

$$
\xi_1:\begin{cases}
\dfrac{\partial C_{11}}{\partial \xi_1}=\dfrac{E_1^{\mathrm{N}}(1-\nu_{12}\nu_{21})+E_1\nu_{12}\partial\nu_{21}}{(1-\nu_{12}\nu_{21})^2}, & \dfrac{\partial C_{12}}{\partial \xi_1}=\dfrac{E_2\nu_{12}^2\partial\nu_{21}}{(1-\nu_{12}\nu_{21})^2}\\
\dfrac{\partial C_{22}}{\partial \xi_1}=\dfrac{E_2\nu_{12}\partial\nu_{21}}{(1-\nu_{12}\nu_{21})^2}, & \dfrac{\partial C_{44}}{\partial \xi_1}=0\\
\dfrac{\partial C_{55}}{\partial \xi_1}=0, & \dfrac{\partial C_{66}}{\partial \xi_1}=0\\
\dfrac{\partial \nu_{21}}{\partial \xi_1}=-\dfrac{m_2m_3}{m_1^2}\dfrac{E_2^{\mathrm{N}}\nu_{12}^{\mathrm{N}}}{E_1^{\mathrm{N}}}
\end{cases}
$$

$$
\xi_2:\begin{cases}
\dfrac{\partial C_{11}}{\partial \xi_2}=\dfrac{E_1\nu_{12}\partial\nu_{21}}{(1-\nu_{12}\nu_{21})^2}, & \dfrac{\partial C_{12}}{\partial \xi_2}=\dfrac{E_2^{\mathrm{N}}\nu_{12}(1-\nu_{12}\nu_{21})+E_2\nu_{12}^2\partial\nu_{21}}{(1-\nu_{12}\nu_{21})^2}\\
\dfrac{\partial C_{22}}{\partial \xi_2}=\dfrac{E_2^{\mathrm{N}}(1-\nu_{12}\nu_{21})+E_2\nu_{12}\partial\nu_{21}}{(1-\nu_{12}\nu_{21})^2}, & \dfrac{\partial C_{44}}{\partial \xi_2}=0\\
\dfrac{\partial C_{55}}{\partial \xi_2}=0, & \dfrac{\partial C_{66}}{\partial \xi_2}=0\\
\dfrac{\partial \nu_{21}}{\partial \xi_2}=\dfrac{m_3}{m_1}\dfrac{E_2^{\mathrm{N}}\nu_{12}^{\mathrm{N}}}{E_1^{\mathrm{N}}}
\end{cases}
$$

$$
\xi_3:\begin{cases}
\dfrac{\partial C_{11}}{\partial \xi_3}=\dfrac{E_1(\nu_{12}^{\mathrm{N}}\nu_{21}+\nu_{12}\partial\nu_{21})}{(1-\nu_{12}\nu_{21})^2}, & \dfrac{\partial C_{12}}{\partial \xi_3}=\dfrac{E_2(\nu_{12}^{\mathrm{N}}+\nu_{12}^2\partial\nu_{21})}{(1-\nu_{12}\nu_{21})^2}\\
\dfrac{\partial C_{22}}{\partial \xi_3}=\dfrac{E_2(\nu_{12}^{\mathrm{N}}\nu_{21}+\nu_{12}\partial\nu_{21})}{(1-\nu_{12}\nu_{21})^2}, & \dfrac{\partial C_{44}}{\partial \xi_3}=0\\
\dfrac{\partial C_{55}}{\partial \xi_3}=0, & \dfrac{\partial C_{66}}{\partial \xi_3}=0\\
\dfrac{\partial \nu_{21}}{\partial \xi_3}=\dfrac{m_2}{m_1}\dfrac{E_2^{\mathrm{N}}\nu_{12}^{\mathrm{N}}}{E_1^{\mathrm{N}}}
\end{cases}
$$

$$
\xi_4:\begin{cases}
\dfrac{\partial C_{11}}{\partial \xi_4}=0, & \dfrac{\partial C_{12}}{\partial \xi_4}=0\\
\dfrac{\partial C_{22}}{\partial \xi_4}=0, & \dfrac{\partial C_{44}}{\partial \xi_4}=G_{23}^{\mathrm{N}}\\
\dfrac{\partial C_{55}}{\partial \xi_4}=0, & \dfrac{\partial C_{66}}{\partial \xi_4}=0
\end{cases}
$$

$$
\xi_5:\begin{cases}
\dfrac{\partial C_{11}}{\partial \xi_5}=0, & \dfrac{\partial C_{12}}{\partial \xi_5}=0\\
\dfrac{\partial C_{22}}{\partial \xi_5}=0, & \dfrac{\partial C_{44}}{\partial \xi_5}=0\\
\dfrac{\partial C_{55}}{\partial \xi_5}=G_{13}^{\mathrm{N}}, & \dfrac{\partial C_{55}}{\partial \xi_5}=0
\end{cases}
$$

$$
\xi_6:\begin{cases}
\dfrac{\partial C_{11}}{\partial \xi_6}=0, & \dfrac{\partial C_{12}}{\partial \xi_6}=0\\
\dfrac{\partial C_{22}}{\partial \xi_6}=0, & \dfrac{\partial C_{44}}{\partial \xi_6}=0\\
\dfrac{\partial C_{55}}{\partial \xi_6}=0, & \dfrac{\partial C_{66}}{\partial \xi_6}=G_{12}^{\mathrm{N}}
\end{cases}
$$

Box I.

References

[1] Sriramula S, Chryssanthopoulos MK. Quantification of uncertainty modelling in stochastic analysis of FRP composites. Composites A 2009;40(11):1673–84.

[2] Sriramula S, Chryssanthopoulos MK. An experimental characterisation of spatial variability in GFRP composite panels. Struct Saf 2013;42:1–11.

[3] Zhou X-Y, Gosling P. Influence of stochastic variations in manufacturing defects on the mechanical performance of textile composites. Compos Struct 2018;194:226–39.

[4] Ben-Tal A, El Ghaoui L, Nemirovski A. Robust optimization. Princeton University Press; 2009.

[5] Acar E, Bayrak G, Jung Y, Lee I, Ramu P, Ravichandran SS. Modeling, analysis, and optimization under uncertainties: a review. Struct Multidiscip Optim 2021;64(5):2909–45.

[6] Zhou X-Y, Ruan X, Gosling P. Robust design optimization of variable angle tow composite plates for maximum buckling load in the presence of uncertainties. Compos Struct 2019;223:110985.

[7] Bacarreza O, Aliabadi M, Apicella A. Robust design and optimization of composite stiffened panels in post-buckling. Struct Multidiscip Optim 2015;51(2):409–22.

[8] Sohouli A, Yildiz M, Suleman A. Efficient strategies for reliability-based design optimization of variable stiffness composite structures. Struct Multidiscip Optim 2018;57(2):689–704.

[9] das Neves Carneiro G, António CC. Reliability-based robust design optimization with the reliability index approach applied to composite laminate structures. Compos Struct 2019;209:844–55.

[10] Duan Z, Jung Y, Yan J, Lee I. Reliability-based multi-scale design optimization of composite frames considering structural compliance and manufacturing constraints. Struct Multidiscip Optim 2020;61(6):2401–21.

[11] Wang L, Liu J, Yang C, Wu D. A novel interval dynamic reliability computation approach for the risk evaluation of vibration active control systems based on PID controllers. Appl Math Model 2021;92:422–46.

[12] Wang L, Liu Y, Li M. Time-dependent reliability-based optimization for structural-topological configuration design under convex-bounded uncertain modeling. Reliab Eng Syst Saf 2022;221:108361.

[13] Wang L, Zhao X, Wu Z, Chen W. Evidence theory-based reliability optimization for cross-scale topological structures with global stress, local displacement, and micro-manufacturing constraints. Struct Multidiscip Optim 2022;65(1):1–30.
[14] Guo X, Bai W, Zhang W. Extreme structural response analysis of truss structures under material uncertainty via linear mixed 0–1 programming. Internat J Numer Methods Engrg 2008;76(3):253–77.
[15] Jansen M, Lombaert G, Schevenels M, Sigmund O. Topology optimization of fail-safe structures using a simplified local damage model. Struct Multidiscip Optim 2014;49(4):657–66.
[16] Zhou M, Fleury R. Fail-safe topology optimization. Struct Multidiscip Optim 2016;54(5):1225–43.
[17] Stolpe M. Fail-safe truss topology optimization. Struct Multidiscip Optim 2019;60(4):1605–18.
[18] Greifenstein J, Stingl M. Topology optimization with worst-case handling of material uncertainties. Struct Multidiscip Optim 2020;61:1377–97.
[19] Thore C-J, Holmberg E, Klarbring A. A general framework for robust topology optimization under load-uncertainty including stress constraints. Comput Methods Appl Mech Eng 2017;319:1–18.
[20] Thore C-J. On a Nash game for topology optimization under load-uncertainity – finding the worst load. In: European congress on computational methods in applied sciences and engineering. 2016.
[21] Sigmund O. On the usefulness of non-gradient approaches in topology optimization. Struct Multidiscip Optim 2011;43.
[22] Sullivan TJ. Introduction to uncertainty quantification, Vol. 63. Springer; 2015.
[23] Kumar D, Koutsawa Y, Rauchs G, Marchi M, Kavka C, Belouettar S. Efficient uncertainty quantification and management in the early stage design of composite applications. Compos Struct 2020;251:112538.
[24] Zhang S, Norato JA. Finding better local optima in topology optimization via tunneling. In: International design engineering technical conferences and computers and information in engineering conference, Vol. 51760. American Society of Mechanical Engineers; 2018, V02BT03A014.
[25] Papadopoulos I, Farrell P, Surowiec T. Computing multiple solutions of topology optimization problems. 2020, arXiv:2004.11797.
[26] Bai S, Kang Z. Robust topology optimization for structures under bounded random loads and material uncertainties. Comput Struct 2021;252:106569.
[27] Hozić D, Thore C-J, Cameron C, Loukil M. A new method for simultaneous material and topology optimization of composite laminate structures using hyperbolic function parametrization. Compos Struct 2021;276:114374.
[28] Reddy JN. Mechanics of laminated composite plates and shells: theory and analysis. CRC Press; 2004.
[29] Lund E. Discrete material and thickness optimization of laminated composite structures including failure criteria. Struct Multidiscip Optim 2018;57(6):2357–75.
[30] Zhang M, Lv H, Kang H, Zhou W, Zhang C. A literature review of failure prediction and analysis methods for composite high-pressure hydrogen storage tanks. Int J Hydrogen Energy 2019;44(47):25777–99.
[31] Tsai SW, Wu EM. A general theory of strength for anisotropic materials. J Compos Mater 1971;5(1):58–80.
[32] Sørensen SN, Lund E. Topology and thickness optimization of laminated composites including manufacturing constraints. Struct Multidiscip Optim 2013;48(2):249–65.
[33] Hughes TJ. The finite element method: linear static and dynamic finite element analysis. Courier Corporation; 2012.
[34] Sørensen SN, Sørensen R, Lund E. DMTO – a method for discrete material and thickness optimization of laminated composite structures. Struct Multidiscip Optim 2014;50(1):25–47.
[35] Kapidžić Z, Nilsson L, Ansell H. Finite element modeling of mechanically fastened composite-aluminum joints in aircraft structures. Compos Struct 2014;109:198–210.
[36] Cook RD, et al. Concepts and applications of finite element analysis. John Wiley & Sons; 2007.
[37] Svanberg K. The method of moving asymptotes—a new method for structural optimization. Internat J Numer Methods Engrg 1987;24(2):359–73.
[38] Svanberg K. A globally convergent version of MMA without linesearch. In: Proceedings of the first world congress of structural and multidisciplinary optimization, Vol. 28. Goslar, Germany; 1995, p. 9–16.
[39] Wächter A, Biegler L. On the implementation of a primal-dual interior point filter line search algorithm for large-scale nonlinear programming. Math Program 2006;106:25–7.
[40] Potra FA, Wright SJ. Interior-point methods. J Comput Appl Math 2000;124(1–2):281–302.
[41] Nocedal J, Wright SJ. Numerical optimization 2nd edition. Springer; 2006, p. 467–80.